ORIGINAL ARTICLE

Journal
the American Ceramic Society

Multifunctional performance of Ti$_2$AlC MAX phase/2D braided alumina fiber laminates

Jesus Gonzalez-Julian[1,2] | Irina Kraleva[3] | Manuel Belmonte[4] | Fabian Jung[5] |
Thomas Gries[5] | Raul Bermejo[3]

[1]Institute of Energy and Climate Research: Materials Synthesis and Processing (IEK-1), Forschungszentrum Jülich GmbH, Jülich, Germany

[2]Department of Ceramics and Refractory Materials, Institute of Mineral Engineering, RWTH Aachen University, Aachen, Germany

[3]Department of Materials Science, Montanuniversität Leoben, Leoben, Austria

[4]Institute of Ceramic and Glass (ICV-CSIC), Madrid, Spain

[5]Institut für Textiltechnik (ITA), RWTH Aachen University, Aachen, Germany

Correspondence
Jesus Gonzalez-Julian, Institute of Energy and Climate Research: Materials Synthesis and Processing (IEK-1), Forschungszentrum Jülich GmbH, Jülich 52425, Germany.
Email: j.gonzalez@fz-juelich.de

Funding information
Germany's Federal Ministry of Education and Research ("Bundesministerium für Bildung und Forschung"), Grant/Award Number: 03SF0534; Spanish Ministry of Science and Innovation (MICINN/AEI) and FEDER (UE), Grant/Award Number: RTI2018-095052-BI00; European Research Council (ERC), Grant/Award Number: 817615

Abstract

The processing and characterization of laminates based on Ti$_2$AlC MAX phase, as matrix, and triaxial alumina braids, as reinforcing phase, are presented. Ti$_2$AlC powders with a mean particle size below 1 μm are synthesized, while commercial 3M Nextel 610 alumina fibers are braided in a three-stage process consisting of spooling, braiding with an angle of 0° and ±60° and the separation to single-layer fabric. The laminates are processed by layer-by-layer stacking, where 3 two-dimensional alumina braids are interleaved between Ti$_2$AlC layers, followed by full densification using a Field-Assisted Sintering Technology/Spark Plasma Sintering. The multifunctional response of the laminates, as well as for the monolithic Ti$_2$AlC, is evaluated, in particular, the thermal and electrical conductivity, the oxidation resistance, and the mechanical response. The laminates exhibit an anisotropic thermal and electrical behavior, and an excellent oxidation resistance at 1200°C in air for a week. A relatively lower characteristic biaxial strength and Weibull modulus (i.e., $\sigma_0 = 590$ MPa and $m = 9$) for the laminate compared to the high values measured in the monolithic Ti$_2$AlC (i.e., $\sigma_0 = 790$ MPa and $m = 29$) indicates the need but also the potential of optimizing MAX-phase layered structures for multifunctional performance.

KEYWORDS
fibers, laminates, MAX phases, strength, Weibull statistics

1 | INTRODUCTION

MAX phases have attracted a considerable attention in the last years due to their unique combination of properties, bridging the gap between ceramics and metals.[1] In general, MAX phases present low density, high elastic modulus, compressive strength and creep resistance as ceramics, and good damage tolerance and

thermal shock resistance, high electrical conductivity, and easily machinability as metals.[2] Furthermore, they present an intermediate coefficient of thermal expansion and good chemical stability with other advanced ceramics and high-temperature superalloys. More than 150 different compositions have been discovered so far, but some aluminum-based MAX phases—mostly Ti_2AlC, Ti_3AlC_2, and Cr_2AlC—have gained more interest due to the excellent oxidation and corrosion resistance up to temperatures around 1300°C.[3] This good oxidation response is caused by the *in situ* formation of an external, thin, well-adhered, and protective α-Al_2O_3 layer.[4] In particular, Ti_2AlC is the most studied and promising composition thanks to the combination of the properties described above, the oxidation cubic kinetics up to temperatures around 1300°C, and availability, non-toxicity, and low cost of the chemical precursors.[5] Based on these features, Ti_2AlC and other Al-MAX phases have been proposed to operate under aggressive environments in different applications such as high-temperature structural material,[6] protective coatings,[7] bond coats in thermal barrier coatings,[8] accident-tolerant fuel cladding in nuclear light water reactors,[9] solar receivers and external walls of the storage tank in concentrated solar power units,[10,11] and as catalyst,[12] among others.[13] However, although Al-MAX phases might be considered for these applications, the aggressive environments demand a unique combination of properties and high degree of reliability in long-term operation, which in some cases Ti_2AlC cannot withstand. Consequently, the most suitable approach to fulfill these requests is to reinforce Ti_2AlC, and in general MAX phases, with secondary phases.

MAX phases have mostly been reinforced with particles in order to improve the hardness and the tribological performance. This approach is successful and relative simple but for a quantitative improvement and tailoring of other properties, continuous fibers would be required. Unfortunately, the number of works is rather limited despite the high potential and interest of these kind of composites. The first consideration to be accomplished is the chemical stability during the processing and in-operando between the fibers and the matrix. Shortly, carbon fibers react with all the MAX-phase compositions, limiting their interest. SiC fibers are suitable for Silicon-based MAX phases (i.e., Ti_3SiC_2) and Al_2O_3 fibers are chemically stable with Aluminum-based MAX Phases (i.e., Ti_2AlC), since typically the "A" element of the MAX phase easily diffuses at high temperature. Nevertheless, the chemical reaction between SiC fibers and Ti_2AlC or Ti_3AlC_2 might be hindered, protecting the fibers with a carbon coating or a thin titanium foil at the interface as diffusion barrier.[14,15] The chemical reaction

is avoided and the mechanical response of the material is improved. Nevertheless, the most realistic approach is to use Ti_2AlC reinforced with alumina fibers, particularly for components that will operate at high temperature under oxidizing environments over long periods of time. In that sense, Ti_2AlC has been reinforced with 20 vol.% of NextelTM-610 and NextelTM-720 alumina fibers.[16] The compressive failure stress in dynamic conditions decreases with increasing temperature, from 1645 MPa at 25°C to 1210 MPa at 1200°C. In addition, compressive fracture strength of $Ti_2AlC/720$ and $Ti_2AlC/610$ composites was enhanced by 39.7% and 32.6% under static loading in comparison with the monolithic Ti_2AlC. These results are promising but further studies are required to analyze the real potential of these composites.

In that sense, the specific adjustment of the fiber–matrix interaction is a great challenge in the development of a damage-tolerant ceramic matrix composite structure. Therefore, the composites characteristics, namely the fiber volume ratio and the fiber orientation, as well as the used reinforcement yarns specifics (amount of yarns being used and the fineness of the roving), have to be defined according to the ceramic application. Within textile processing, these reinforcement characteristics can be set by choosing the manufacturing process employed for the production of semi-finished textiles. Established textile processes for the production of continuous fiber reinforcement structures are weaving, tape laying, and braiding. Among these technologies, braiding holds a high potential to generate the reinforcements to be used for the production of high-performance components due to its ability to create load adjusted and complex surface area as well as volume-forming structures (e.g., through three-dimensional [3D] braiding).

In the braiding process, a fiber reinforcement structure is primarily created by the regular crossing of at least three braiding yarns that run diagonally to the production direction (possible variation of braiding angle: $0° < \alpha < 90°$).[17] With the diagonal intersection of the braiding yarns along the production direction, a fabric is created, consisting of braiding yarns oriented in two linear directions. Therefore, these braided fabrics are defined as biaxial-oriented braids. Furthermore, axial reinforcement fibers, so-called inlay yarns or 0°-yarns, can be integrated into the braid parallel to the production direction. Consequently, in contrast to weaving, braiding can be used to produce triaxial-oriented semi-finished textiles.[18,19] In addition to textile processes like fiber layup or automated fiber placement, braiding allows the production of unidirectionally (UD) oriented fabrics. Therefore, so-called UD braids are processed by interlacing braiding and supporting yarns.[20,21] Since the supporting yarns are defined by a significantly

lower fiber fineness (fineness measured in denier: 1 den =1 g/9000 m) compared to the braiding yarns, the vertical fiber ondulation induced by the fiber crossovers can be eliminated. Load-bearing braiding yarns are thus stretched and oriented in one direction and form a stable semi-finished textile structure.

The aim of this work is to develop multifunctional laminates composed of Ti_2AlC containing two-dimensional (2D) braided alumina fibers. Braiding of the continuous alumina fibers, processing of the laminates, densification by Spark Plasma Sintering, and microstructural characterization are presented. Furthermore, the multifunctional response of the developed composites is investigated, including the electrical, thermal, and mechanical properties, as well as the oxidation resistance at high temperature.

2 | EXPERIMENTAL PROCEDURE

2.1 | Processing and materials

Ti_2AlC powders were synthesized by molten salt shielded synthesis method, following the same procedure as described elsewhere.[22] Ti (−325 mesh, 99.5%; Alfa Aesar), Al (−325 mesh, 99.5%; Alfa Aesar), and graphite (APS 7–11 µm, 99%; Alfa Aesar) powders were mixed in a molar ratio of 2:1:0.9, respectively. KBr (99%; Alfa Aesar) was used as salt and mixed with the starting precursors in a 1:1 weight ratio employing a 3D shaker mixer (Turbula; Bachofen AG), ethanol as liquid media and zirconia balls for 24 h. Afterwards, the mixture was dried in a rotary evaporator and sieved through a 300-µm mesh. The resultant powder was uniaxially pressed at 100 MPa, placing the pellets into a cylindrical alumina crucible and filling the empty space with extra KBr. The alumina crucibles were introduced into an open furnace and heated at 5 K min^{-1} up to 1000°C, which was held for 5 h. After cooling, the crucible was washed in hot water and the pellets were boiled in deionized water. Then, the MAX powders were vacuum filtrated and washed with deionized water and ethanol. Finally, the powders were dried in an oven at 70°C overnight and sieved through a 25-µm sieve.

The laminates were reinforced by triaxial braided alumina fibers. Accordingly, the braids were manufactured in a three-stage process consisting of spooling the alumina fiber on modified braiding bobbins, cable for the processing of brittle fiber materials. It was followed by the production of the reinforcing textile by 2D braiding and the separation of the triaxial braid into stackable individual layers. In the preparation for the braiding process, the alumina fiber rovings type 3M Nextel 610 (α-Al_2O_3; filament diameter of 10–12 µm and fineness of 3000 denier) were used once they were separated from the master spool (transport carrier) by a semi-automatic spooling machine (SP 280; August Herzog Maschinenfabrik GmbH & Co. KG). Using a spooling speed of 0.2 m s^{-1}, bobbins were prepared, each holding 25 or 55 m alumina fiber according to form braiding or inlay yarns. Afterwards, they were transferred into a radial braiding machine (RF 1/144-100; August Herzog Maschinenfabrik GmbH & Co. KG), and a bobbin set of 96 braiding yarns and 36 inlay yarns were used to produce the triaxial textile. The braiding process was performed at a takeoff speed of 0.001 m s^{-1} onto a cylindrical PTFE braiding core with a diameter of 75 mm. The braid was guided by a braiding ring with an inner diameter of 100 mm. According to the selected parameters, the braiding yarns were aligned to a braiding angle (α) of 0° and ±60° to form a triaxial-oriented circumferential braid on the braiding core. Following the braiding process, the textile was lifted from the core and cut open parallel to the longitudinal axis of the braid. Afterwards, the separated individual layers were stored at room temperature prior being stacked with the Ti_2AlC powder to form the laminate.

The Ti_2AlC/Al_2O_{3f} laminates were sintered using a Field-Assisted Sintering Technology/Spark Plasma Sintering (FAST/SPS, FCT-HPD5; FCT Systeme GmbH). The powders were poured into a graphite tool with inner diameter of 20 mm following a layer-by-layer stacking, which allows an easy control of the number, location, and thickness of the different layers. First, Ti_2AlC powder was poured and uniaxially pressed at 5 MPa to obtain the first powder layer. Then, a 2D braided alumina textile, consisting of fiber rovings of 20 mm diameter, was placed on top of the Ti_2AlC layer, followed by pouring another Ti_2AlC layer of powder and pressing at 5 MPa. This process of layer-by-layer stacking leads to easily control the number of layers and thicknesses. In our case, laminates containing three 2D braided alumina textiles were processed. Accordingly, laminates were fabricated by embedding three alumina braids in a symmetric multilayer configuration, placing the alumina fiber braids at ~500 µm from each another. The sintering conditions were a heating rate of 100 K min^{-1}, maximal temperature of 1200°C, dwell time of 10 min, uniaxial pressure of 50 MPa, and vacuum (~4 mbar) during the whole thermal cycle. Temperature was controlled using a pyrometer that was focused on the surface of a drilled punch at only 5 mm from the powder. Bulk Ti_2AlC specimens were processed and sintered using the same parameters for reference purposes. After sintering, both monolithic and laminate samples with 20 mm diameter were ground on both sides, reaching a final thickness of 1.2 and 1.4 mm for the monolithic Ti_2AlC and laminate materials, respectively.

2.2 | Microstructural characterization, electrical and thermal properties, and oxidation response

Density of the samples was measured by Archimedes method in water at room temperature. Crystal phases were identified by X-ray diffraction (D4-Endeavor; Bruker AXS) over the 2θ range of 10º and 80º, a step size of 0.02°, and dwell time of 0.5 s/step. Fracture surfaces and polished cross sections were observed in a Scanning Electron Microscope (SEM; Zeiss Ultra55). The effective electrical conductivity in the parallel (σ_{par}) and perpendicular (σ_{per}) directions to the laminates was determined in prismatic bars by the four-probe DC method (potentiostat/galvanostat; Autolab PGSTAT302N) and a current flow ranging from 40 to 3000 mA. The thermal diffusivity of square reference and laminate specimens of 8.8 x 8.8 mm^2 and 0.5–1.0 mm of thickness was measured as a function of the temperature in the parallel direction to the SPS pressing axis (perpendicular in the case of laminates, also known as through-thickness direction) by the laser-flash method (Thermaflash 2200; Holometrix Netzsch). The experiment in the perpendicular direction was not performed due to the difficulties to machine a sample with 0.5 mm of thickness containing at least one alumina layer within the bulk and being perfectly aligned to the outer surfaces of the specimen. The thermal conductivity (kt) was assessed known the density (ρ) of the specimen, the thermal diffusivity (α), and the specific heat capacity (Cp), according to the following equation: kt = $\rho \cdot \alpha \cdot$ Cp. The evolution of the parameter Cp with the temperature for the reference Ti$_2$AlC material was estimated using data collected by Wang et al.,[23] while in the case of laminates, Cp was calculated by the rule of mixtures, also using heat capacity data for α-Al$_2$O$_3$ taken from the NIST-JANAF database, considering a total content of Al$_2$O$_{3f}$ into the laminates of 11.8 wt.%. The oxidation response of the laminates was performed introducing the samples into an oven at 1200°C for 1 week. Afterwards, the samples were perpendicularly cut, mounted, polished with 0.5-μm diamond paste, and observed by SEM.

2.3 | Evaluation of the mechanical properties

For the evaluation of the Vickers Hardness (HV), a top and a side surface of several Ti$_2$AlC monolithic and Ti$_2$AlC/Al$_2$O$_{3f}$ laminate specimens were prepared, polishing to a 1-μm mirror finish for a better imprint identification of the indent. Loads of 1 and 3 kg were applied on both surfaces using a pyramid-shaped diamond Vickers indenter using an indenter machine (Zwick 3212001; ZwickRoell

GmbH & Co. KG). For statistical significance, 10 indents were performed for each load at each polished surface for each material. The corresponding Vickers Hardness was evaluated according to the EN 843-4 standards.[24] The mechanical strength of the Ti$_2$AlC monolithic and Ti$_2$AlC/Al$_2$O$_{3f}$ laminate samples was evaluated under biaxial bending, using the Ball-on-Three-Balls (B3B) testing method.[25,26] In the B3B testing setup, one side of a disc (or plate)-shaped specimen is symmetrically supported by three balls, the other side is loaded at the midpoint of the specimen through a fourth ball. During testing setup, a defined pre-load is applied to guarantee contact between balls and specimen. Subsequently, the applied force is constantly increased until fracture of the specimen is registered. Due to the fact that during the B3B test only a small effective area or volume in the center of the specimen is under biaxial stress, the influence of edge defects may be neglected; this avoids possible failure of specimens from chamfered edges, which would influence the measurement of the "real" material strength distribution.

All B3B tests were performed using a universal testing machine (Zwick Z010; Zwick-Roell GmbH & Co. KG) with a load cell of 10 kN, a selected pre-load of 10 N and a displacement rate of 0.7 mm min^{-1} in ambient conditions (23°C and ~22% relative humidity). The diameter of the supporting balls as well as loading ball was chosen to be 15.08 mm. A total of 10 disc-shaped specimens per set (monolith and laminate) were tested. Fractography was carried out on broken specimens to identify the fracture origin and location of critical flaws in both monolithic and laminate samples. Selected fracture surfaces were sputtered with gold using an Agrar Sputter Coater and observed by SEM (JEOL JCM-6000Plus; NeoscopeTM, JEOL Ltd.).

3 | RESULTS AND DISCUSSIONS

3.1 | Processing and microstructural characterization

The first step to develop laminates is the processing of the 2D braided fabrics (Figure 1). The fiber architecture and the fiber–matrix interface dictate the final response, which is defined by the selection of fiber quality and textile processing. At the roving level (1D), for example, the specific contact area of the individual fiber filaments can be enlarged by increasing the fiber fineness. Respectively, an increase in the number of threads can be implemented at the level of the textile surface (2D). Likewise, an increase of the interaction area can be achieved by maximizing the number of selected reinforcing layers in the (3D) spatial composite. In that sense, by creating a defined triaxial braid (Figure 1), composed of oriented fibers at angles of 0° and ±60°, the
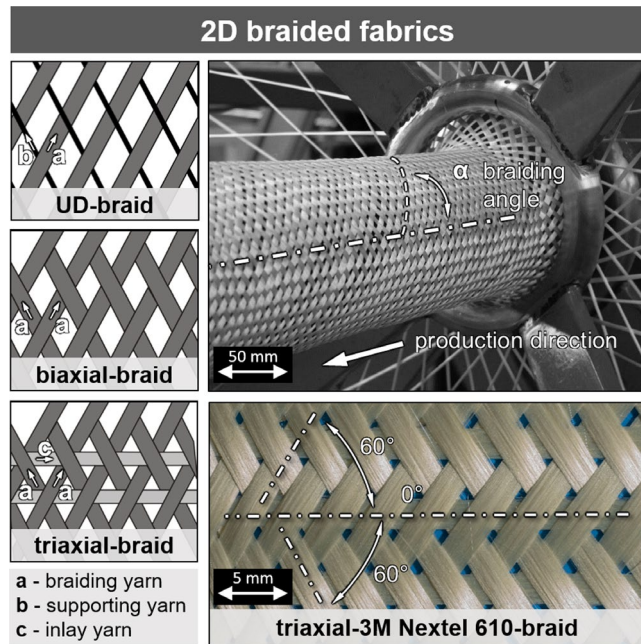
FIGURE 1 Processing, design, and angles of the two-dimensional alumina fiber braids

structural mechanics of the fiber reinforcement are homogenized, eliminating the direction-dependent effect within the fabrics. This configuration results in a reinforcement, defined by quasi-isotropic mechanical properties of the individual braided layers. In the context of the development of continuous fiber-reinforced Ti_2AlC/Al_2O_{3f}, it is necessary to investigate suitable lightweight design specifications for the composite material. Here, 2D braiding offers a wide range of possibilities for the production of composite-specific reinforcement textiles due to its high degree of variation with regard to the orientation of the reinforcing fibers. The second step is to define the number and thickness of the layers, which is easy to assess by the versatility of the layer-by-layer stacking method. In the current work, just one configuration containing three 2D alumina braids between the Ti_2AlC layers was processed and characterized, although a sample incorporating four alumina fiber layers was also produced as a proof of concept. Finally, the third step is the densification of the laminate, which was carried out in a FAST/SPS in order to fully densify the samples, control the phase purity, and limit the grain growth, as reported in a previous work.[22]

FIGURE 2 Photographs of the Ti_2AlC/Al_2O_{3f} laminates after (A) sintering and (B) breaking. (C–G) SEM micrographs of the fracture surface at different magnifications and locations. SEM, scanning electron microscope
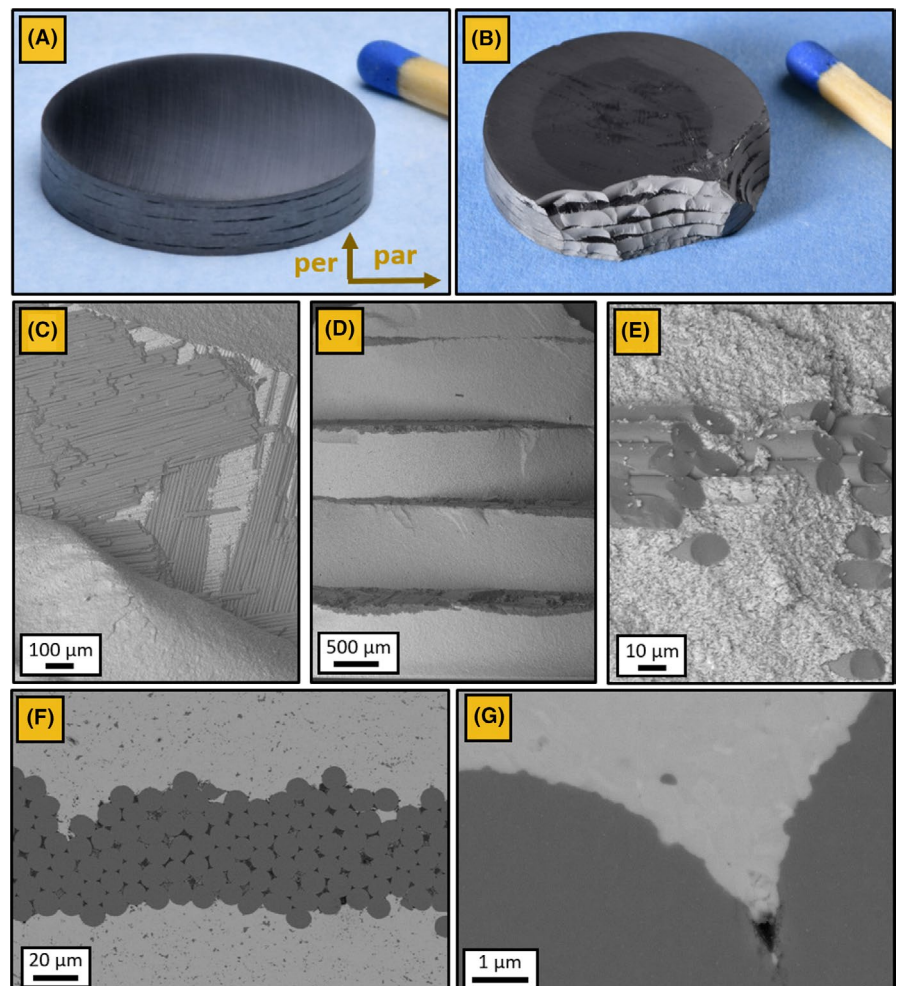
After sintering, the monolithic material and the Ti_2AlC/Al_2O_{3f} laminate present high density, specifically 99.9% of the theoretical density, and no cracks, flaws, or delamination were detected in the laminate (Figure 2A). This is caused by different reasons, where one of the most determinant is the coefficient of the thermal expansion (CTE) match between the alumina Nextel610 fibers (7.9 x 10^{-6} K^{-1}) and Ti_2AlC (8.2 x 10^{-6} K^{-1}), which strongly reduces the thermal stresses. The sample was broken and a stepped fracture surface is observed, which might indicate different reinforcing mechanisms such as crack deflection and pull-out (Figure 2B,C). The different Ti_2AlC layers and 2D alumina braids are easily observed in the fracture surface (Figure 2D). Certainly, the alumina braids are continuous and separate the different Ti_2AlC layers. However, at some locations, Ti_2AlC grains can be observed between fibers (Figure 2E) and even connecting two different MAX-phase layers (Figure 2D). This might have some consequences in the thermal and mechanical, and particularly, the electrical response. As expected, no reaction between the fibers and the matrix was observed as no secondary phases were observed at the interface (Figure 2F,G). This lack of reactions is based on different factors such as the low temperature of the processing, the short dwell time during sintering, and the potential inward and outward diffusion of the same cation (Al^{3+}) from the fibers and matrix.

3.2 | Electrical and thermal properties and oxidation resistance

Table 1 shows the density of the Ti_2AlC/Al_2O_{3f} laminate and the reference specimen as well as the electrical and thermal conductivity on both directions, parallel and perpendicular to the 2D braids. One of the main advantages of developing MAX-phase laminates is the possibility to produce highly anisotropic MAX-phase compounds, as, for example, an outstanding electrical conductor in one direction while insulator in the other. The electrical conductivity on the parallel direction of the laminate is $1.5 \cdot 10^6$ S m^{-1}, which is a similar value to that reported in the literature for Ti_2AlC,[27] as was expected since in this direction the conduction is controlled by the Ti_2AlC matrix. However, in the direction perpendicular to the braids, the Ti_2AlC conductive layers are separated by alumina braids,

which are electrical insulators. Consequently, low electrical conductivity might be expected in this orientation. An electrical conductivity of $2.2 \cdot 10^4$ S m^{-1} was measured, which is two orders of magnitude lower than in the parallel direction but still a relatively high conductivity value. As described before, the insulator alumina braids mostly keep separate the electrical conductor Ti_2AlC layers, but at some locations the separation is disrupted (Figure 2D,E), allowing the electrical current flows at those points. As result, the overall electrical conductivity in the perpendicular direction decreases due to the braids, although the lack of continuous and uniform insulating barriers avoids to fully convert the composite into an electrical insulator material in that direction.

Figure 3 collects the evolution of the thermal parameters with the temperature for the monolithic Ti_2AlC and the laminate. In this way, both materials exhibit a continuous increment in the specific heat capacity, Cp, over the temperature (Figure 3A). The laminate shows a higher value than the monolithic material in the whole range of temperatures, associated with the contribution of the alumina fibers that have a higher Cp. Conversely, α (Figure 3B) is slightly larger at room temperature for the reference material (0.11 cm^2 s^{-1}) than for the laminate (0.10 cm^2 s^{-1}), widening that difference as the temperature increases. A similar trend is observed with the thermal conductivity, when kt is plotted (Figure 3C). In fact, the conductivity of the monolithic Ti_2AlC at room temperature is 26.5 W m^{-1} K^{-1}, in good agreement with values reported by other authors,[28] whereas kt for the laminate is 24.9 W m^{-1} K^{-1}. As the temperature increases that difference is enlarged (up to 50% at 1073 K), keeping kt almost constant in the reference material. Considering that the microstructural characteristics, mainly the grain size, of Ti_2AlC in the monolithic material and the laminate are similar, the lower thermal conductivity measured for the laminate would be explained by a larger contribution of the phonon scattering process that would preferentially take place at the interface between the alumina braids and the Ti_2AlC matrix as well as between the fibers forming the braids.

Figure 4 shows the polished cross section of the Ti_2AlC/Al_2O_{3f} laminate after the oxidation at 1200°C for 168 h, which corresponds to a whole week. On top of the Ti_2AlC matrix, an external and continuous α-Al_2O_3 layer is in situ formed during the oxidation, which is decorated

TABLE 1 Density, theoretical density, and electrical and thermal conductivities of the different materials in the parallel (par) and perpendicular (per) direction to the alumina braids

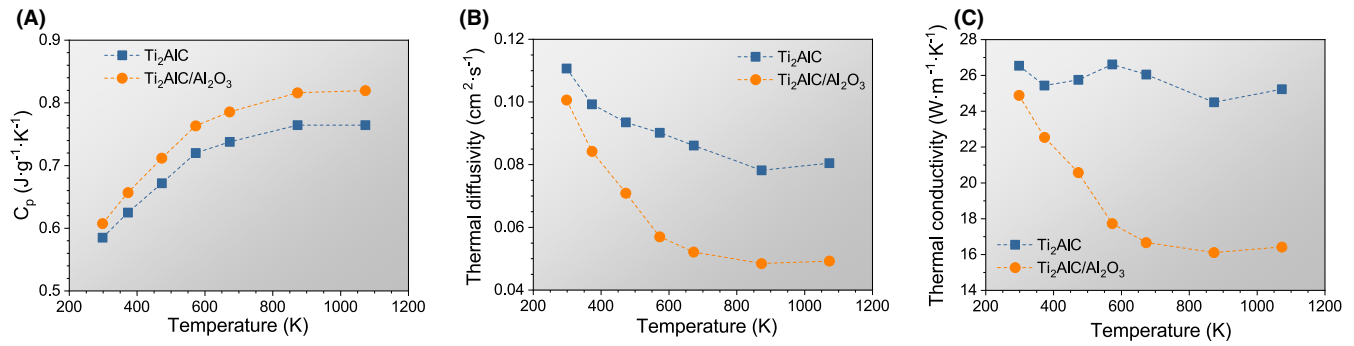| Sample	Density (g cm^{-3})	Theor. density (%)	σ_{par} (S m^{-1})	σ_{per} (S m^{-1})	kt_{par} (W m^{-1} K^{-1})	kt_{per} (W m^{-1} K^{-1})
Ti_2AlC	4.094	99.9			33.9	26.5
Ti_2AlC/Al_2O_3	4.073	99.9	$1.5 \cdot 10^6$	$2.2 \cdot 10^4$	30.9	24.5

(A)

(B)

(C)

FIGURE 3 (A) Specific heat capacity, (B) thermal diffusivity, and (C) thermal conductivity of the monolithic Ti_2AlC and Ti_2AlC/Al_2O_{3f} laminate in the range of temperature from 273 to 1073 K

FIGURE 4 SEM micrographs of polished cross sections of the laminate after oxidation at 1200°C for 168 h at (A) top surface and (B) Ti_2AlC/alumina braids interface. SEM, scanning electron microscope
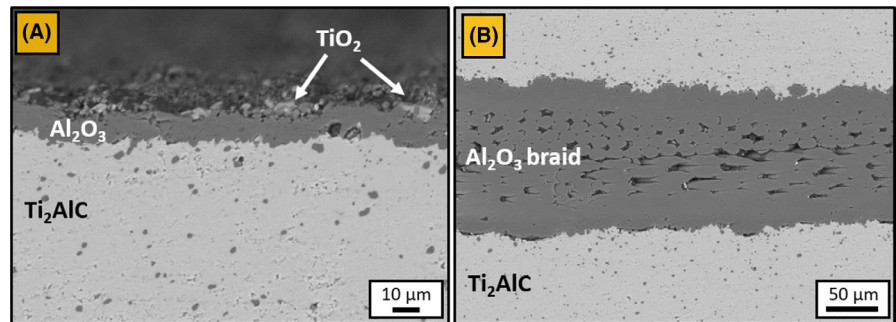
with small TiO_2 particles (Figure 4A). The alumina layer presents a uniform thickness of ~10 μm, which is in good agreement with the reported values in the literature and responsible of the good oxidation resistance.[29,30] No other phases were detected, particularly at the interface between Ti_2AlC and the Al_2O_3 layer, and importantly, a strong adhesion of the Al_2O_3 layer is presumed since no cracks or delamination are observed. The interface between the alumina braids and the Ti_2AlC matrix is shown in Figure 4B. As expected, no other phases were detected because of the chemical stability and compatibility between both compositions. Furthermore, no cracks and/or delamination were detected, which is correlated once again with the CTE match between both materials.[31]

3.3 | Hardness and biaxial strength distribution

The hardness evaluated in the Ti_2AlC phase on both top and side surfaces of the monolithic material and Ti_2AlC/Al_2O_{3f} laminates was similar, with values of ~8.0 GPa ± 0.2, showing no significant effect of the indent location. No significant difference in hardness was also found between HV1 and HV3. Figure 5 shows representative examples of 1 and 3 kg indents on both a Ti_2AlC sample and on the central Ti_2AlC layer of the laminate. At loads below 1 kg, no cracks were detected in the monolithic and laminate samples. This

phenomenon is characteristic of MAX-phase compounds, where the energy is absorbed in the nearby area of the indentation. However, cracks emanating from the 3 kg indents can be observed in both materials, indicating the relatively brittle behavior of the Ti_2AlC phase, associated with the very small grain size. It is worth pointing out that the reported HV1 hardness of 8.3 ± 0.2 GPa (Table 2) is relatively high for MAX phases, and may be related to the sub-micron grain size of the material.[22]

Our hypothesis on how to improve the mechanical response of MAX phases by using braiding fibers embedded between the MAX layers is based on previous investigations by some of the authors and the literature.[32,33] The idea is to exploit the potential of in-plane residual stresses (due to CTE mismatch) and weak interfaces to either arrest the propagation of surface cracks or deflect and guide the crack within the layer containing the braided fibers. The biaxial strength, σ_f, for Ti_2AlC monolithic and Ti_2AlC/Al_2O_{3f} laminate samples tested under B3B was evaluated for every specimen according to:

$$\sigma_f = f\left(\frac{t}{R}, \frac{R_a}{R}, \nu\right) * \frac{F}{t^2} \qquad (1)$$

where F is the maximum load at fracture in [N], and t is the thickness of the specimen in [mm]. In the case of (isotropic) disc-shaped specimens, the dimensionless factor f has been evaluated for a wide parameter set and is only dependent on

the support geometry (R_a/R), the specimen geometry (t/R), and the Poisson's ratio ν of the material (see Ref. [25] for more details). Assuming a Poisson's ratio of $\nu = 0.19$ for the Ti$_2$AlC material, and an average thickness of ~1.3 mm for monolithic and laminate specimens, a factor $f \approx 1.7$ can be calculated.

Figure 6 represents the strength distribution of Ti$_2$AlC monolithic and Ti$_2$AlC/Al$_2$O$_{3f}$ laminate samples in a Weibull diagram. The probability of failure, P, is plotted versus the failure stress, s_f, calculated for every specimen according to Equation (1).

The strength data were evaluated in the framework of the Weibull statistics[34] following the EN-843-5 standard. The probability of failure as a function of the applied stress can be described using a 2-parameter Weibull distribution, as according to:

$$P(\sigma_{appl}) = 1 - \exp\left[-\left(\frac{\sigma_f}{\sigma_0}\right)^m\right] \quad (2)$$

The characteristic strength, σ_0, represents the applied stress associated with a ~63% probability of failure. The

Weibull modulus, m, describes the width of the strength distribution and indicates the scatter of the size of the critical defects in the sample. The dashed lines in Figure 6 represent the best fit of the strength data sets, for both samples, according to the maximum-likelihood method.[34] Although only 10 specimens per sample were tested, evaluation of Weibull parameters (i.e., characteristic strength, σ_0, and Weibull modulus, m) was performed for comparative purposes. The corresponding Weibull parameters for the monolithic Ti$_2$AlC and the Ti$_2$AlC/Al$_2$O$_{3f}$ laminate samples along with the corresponding 90% confidence intervals are given in Table 2.

A relatively high characteristic strength ($\sigma_0 = 790$ MPa) was measured for the Ti$_2$AlC monolithic sample, compared to flexural strength of ~300 MPa, as reported in the literature for the MAX-phase material.[35] To our knowledge, and according to the literature, the strength reported here is the highest strength measured in a MAX phase so far.[36] Beyond the high strength, it is worth highlighting the high Weibull modulus ($m = 29$) of the Ti$_2$AlC monolithic sample, which is related to the narrow critical defect size population in the material, and may be associated
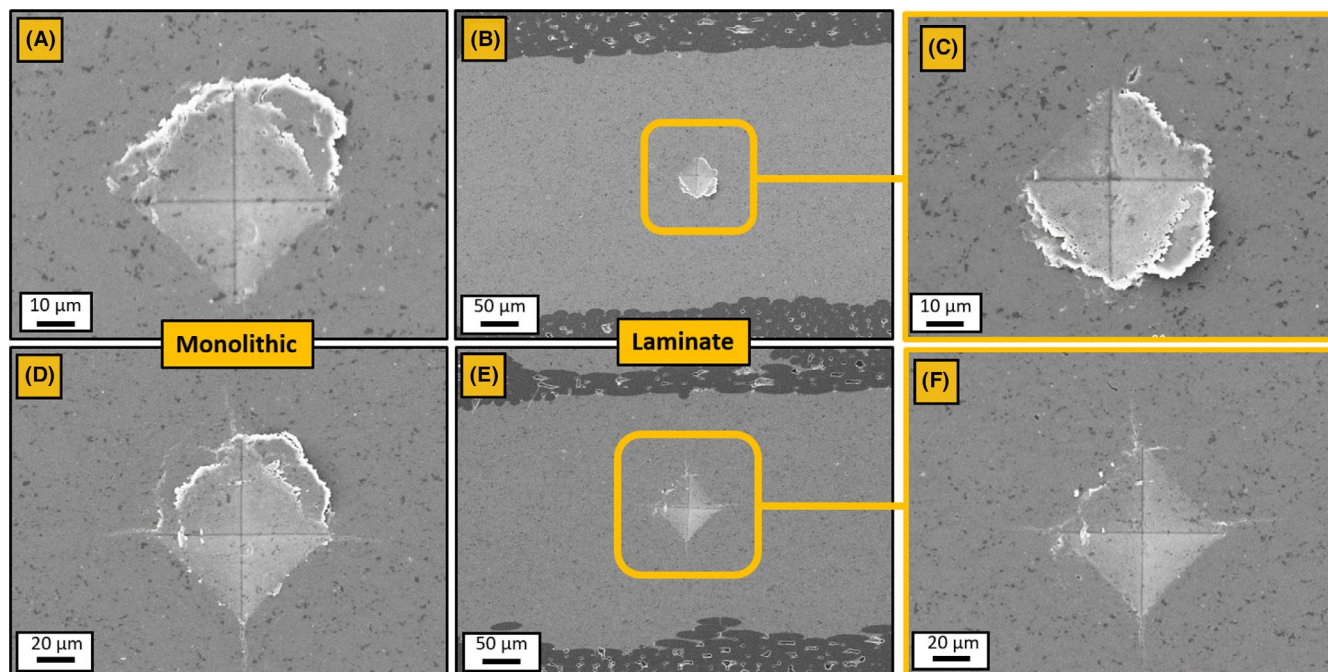

FIGURE 5 SEM micrographs of the Vickers indentations at (A–C) 1 and (D–F) 3 kg. SEM, scanning electron microscope

TABLE 2 Vickers Hardness at 1 and 3 kg, characteristic strength at room temperature, and Weibull modulus of the monolithic and laminate samples

Sample	HV1 (GPa)	HV3 (GPa)	Characteristic strength (MPa)	Weibull (−)
Ti$_2$AlC	7.7 ± 0.2	7.8 ± 0.4	790 [773–808]	29[16–39]
Ti$_2$AlC/Al$_2$O$_3$	8.3 ± 0.2	8.2 ± 0.1	530 [492–572]	9 [5–12]

with certain damage tolerance behavior, as evidenced by this type of material. On the other hand, the characteristic strength of the Ti_2AlC/Al_2O_{3f} laminate was lower

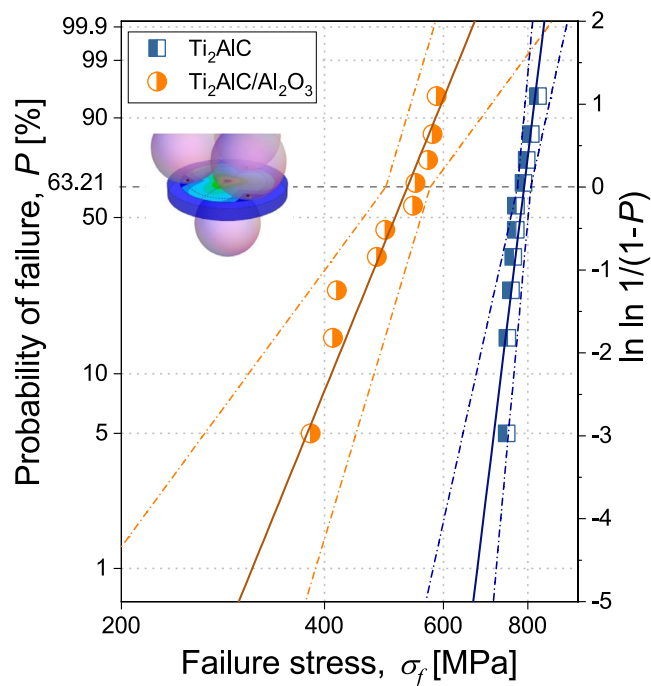**FIGURE 6** Strength distributions of the Ti_2AlC monolithic and Ti_2AlC/Al_2O_{3f} laminate tested using the B3B method. The straight lines represent the best fit of a 2-parameter Weibull distribution, and the dashed lines represent the corresponding 90% confident intervals

($\sigma_0 = 530$ MPa), compared to the monolithic counterpart, with a rather low Weibull modulus ($m = 9$). This suggests a different failure mechanism in the latter.

3.4 | Failure analysis of monoliths and laminates

Figure 7 shows representative broken specimens for the monolithic and laminate samples after B3B testing. Figure 7A,D illustrate a top view of a monolith and laminate, respectively, with different number of broken parts, associated with the stored energy during the test. Higher failure stress can be related to larger number of pieces, in our case corresponding to the monolithic MAX phase. The corresponding fracture surfaces are illustrated in Figure B,C,E, and F, with the failure origin located at the tensile surface. In case of monolithic Ti_2AlC, no pores or large grains could be found, indicating good quality microstructural processing through SPS. In the case of the multilayer samples, braided alumina were found to be the common source of failure in the samples, with the fibers being located at or near the tensile surface. In addition, fracture through the fibers, with no signs of delamination, was mainly observed. These findings point out the need of improving the processing of the layered structures, which is ongoing work. In this regard, and based on previous works on Al_2O_3-layered ceramics,[32] the location of the alumina braids should be relative close to both surfaces,
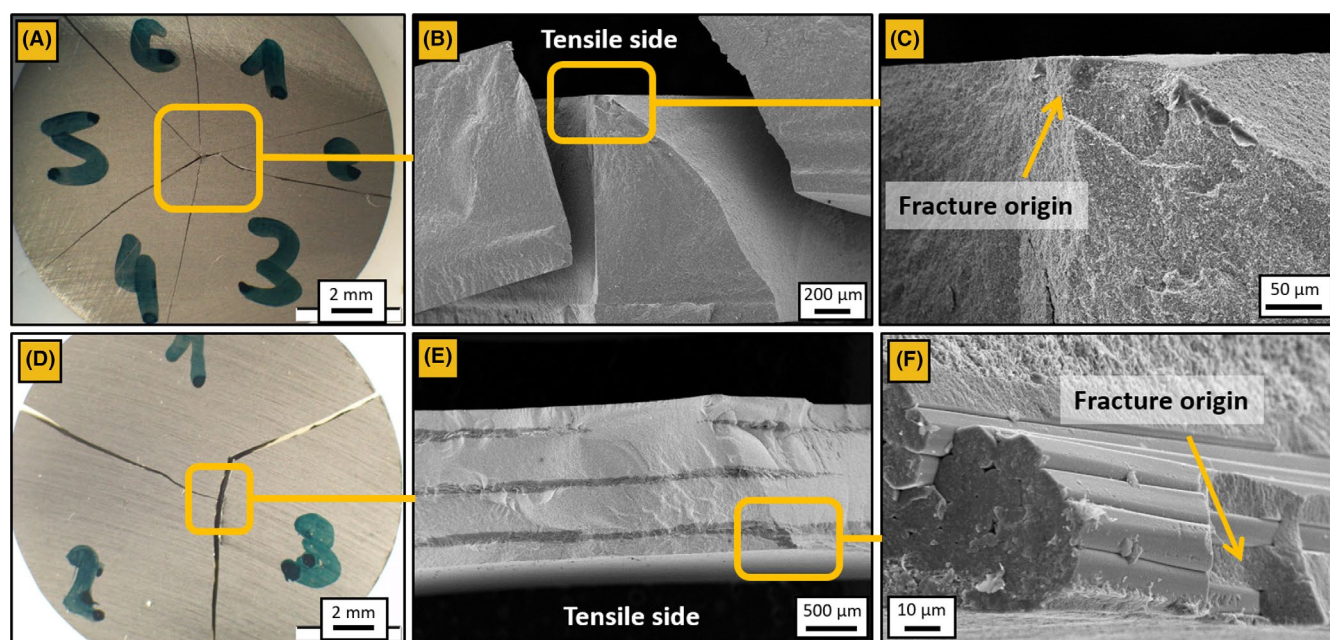

FIGURE 7 Top view of a broken specimen corresponding to (A) Ti_2AlC monolithic and (D) Ti_2AlC/Al_2O_{3f} laminate samples. (B,C,E,F) SEM micrographs of fracture origins in monolithic and laminate specimen, respectively

to be effective against the propagation of surface flaws (cracks). However, fibers connecting the surface (as those found in this work) may act as stress concentrators, thus lowering the mechanical strength. Importantly, almost no reinforced mechanisms were observed (Figures 2E and 7E) at the matrix/fiber interface such as deflection and/or pull out. The matrix/fiber interface plays a determinant role to arrest and/or deflect cracks, thus its control through thin coatings on the fibers or other strategies such as some porosity should be investigated in the near future to improve the mechanical response of MAX-phase-based materials for high temperature applications.

4 | CONCLUSIONS

In this work, symmetric laminates consisting of three 2D alumina braids among four Ti_2AlC layers were designed and fabricated using the simple layer-by-layer stacking and a FAST/SPS. Laminates were fully densified (99.9% of the theoretical density) and no reaction or delamination was detected at the interface between the matrix and the fibers due to chemical stability and compatibility, and the good CTE match. The electrical conductivity of the Ti_2AlC/Al_2O_{3f} laminates exhibits an anisotropic respond, being two orders of magnitude larger in the plane parallel to the alumina braids ($1.5 \cdot 10^6$ S m^{-1}) than in the perpendicular direction. The thermal conductivity in the laminate at room temperature is 25 W m^{-1} K^{-1} in the plane perpendicular to the braids, similar to that of the monolithic Ti_2AlC, and drops with the temperature reaching ~16 W m^{-1} K^{-1} at 1073 K. The oxidation response at 1200°C in air of the laminates is similar to that found for Ti_2AlC, consisting of a thin and well-adhered alumina layer protecting against further oxidation. A very high hardness of the monolithic and laminate samples around 8 GPa was measured, which may be associated with the small grain size (<1 μm) of the Ti_2AlC material. The characteristic biaxial strength of Ti_2AlC is the highest reported so far ($\sigma_0 = 790$ MPa), with a very high Weibull Modulus ($m = 29$). The incorporation of the fibers in the laminate does not increase the characteristic strength of the material because they are located at or near the tensile surface, acting as the origin of the fracture. This reveals the importance of the location, number of layers, and their thickness in order to improve the mechanical response of MAX-phase laminates, while tailoring the thermal and electrical properties. Importantly, the matrix/fiber interface should also be tailored, using for example thin coatings, in order to arrest and/or deflect cracks and to promote reinforced mechanisms such as fiber pull out.

ORCID

Jesus Gonzalez-Julian https://orcid.org/0000-0002-4217-8419
Manuel Belmonte https://orcid.org/0000-0001-6668-6920
Fabian Jung https://orcid.org/0000-0002-9677-5171
Raul Bermejo https://orcid.org/0000-0002-6891-3653

REFERENCES

1. Radovic BM, Barsoum MW. MAX phases: bridging the gap between metals and ceramics. Am Ceram Soc Bull. 2013;92(3):20–7.
2. Barsoum MW. MAX phases: properties of machinable ternary carbides and nitrides. Weinheim: Wiley VCH; 2013.
3. Smialek JL. Oxygen diffusivity in alumina scales grown on Al-MAX phases. Corros Sci. 2015;91:281–6.
4. Yu W, Vallet M, Levraut B, Gauthier-Brunet V, Dubois S. Oxidation mechanisms in bulk Ti_2AlC: influence of the grain size. J Eur Ceram Soc. 2020;40(5):1820–8.
5. Tallman DJ, Anasori B, Barsoum MW. A critical review of the oxidation of Ti_2AlC, Ti_3AlC_2 and Cr_2AlC in air. Mater Res Lett. 2013;1(3):115–25.
6. Smialek JL, Harder BJ, Garg A. Oxidative durability of TBCs on Ti_2AlC MAX phase substrates. Surf Coatings Technol. 2016;285:77–86.
7. Smialek JL, Nesbitt JA, Gabb TP, Garg A, Miller RA. Hot corrosion and low cycle fatigue of a Cr_2AlC-coated superalloy. Mater Sci Eng A. 2018;711:119–29.
8. Gonzalez-Julian J, Mauer G, Sebold D, Mack DE, Vassen R. Cr_2AlC MAX phase as bond coat for thermal barrier coatings: processing, testing under thermal gradient loading, and future challenges. J Am Ceram Soc. 2020;103:2362–75.
9. Murty KL, Charit I. Structural materials for Gen-IV nuclear reactors: challenges and opportunities. J Nucl Mater. 2008;383:189–95.
10. Sarwar J, Shrouf T, Srinivasa A, Gao H, Radovic M, Kakosimos K. Characterization of thermal performance, flux transmission performance and optical properties of MAX phase materials under concentrated solar irradiation. Sol Energy Mater Sol Cells. 2018;182:76–91.

11. Van Loo K, Lapauw T, Ozalp N, Ström E, Lambrinou K, Vleugels J. Compatibility of SiC-and MAX phase-based ceramics with a KNO_3-$NaNO_3$ molten solar salt. Sol Energy Mater Sol Cells. 2019;195:228–40.

12. Trandafir MM, Neaţu F, Chirica IM, Neaţu Ş, Kuncser AC, Cucolea EI, et al. Highly efficient ultralow Pd loading supported on MAX phases for chemoselective hydrogenation. ACS Catal. 2020;10(10):5899–908.

13. Gonzalez-Julian J. Processing of MAX phases: from synthesis to applications. J Am Ceram Soc. 2021;104:659–90.

14. Guo S, Hu C, Gao H, Tanaka Y, Kagawa Y. SiC(SCS-6) fiber-reinforced Ti_3AlC_2 matrix composites: interfacial characterization and mechanical behavior. J Eur Ceram Soc. 2015;35(5):1375–84.

15. Guo S. Improvement of mechanical properties of SiC(SCS-6) fiber-reinforced Ti_3AlC_2 matrix composites with Ti barrier layer. J Eur Ceram Soc. 2015;36:1349–58.

16. Parrikar PN, Gao H, Radovic M & Shukla A Static and dynamic thermo-mechanical behavior of Ti2AlC MAX phase and fiber reinforced Ti2AlC composites. Dynamic behavior of materials. In: Conference Proceedings of the Society for Experimental Mechanics Series; 2015. p. 9–14.

17. Kyosev Y. Braiding technology for textiles: principles, design and processes. Sawston: Woodhead Publishing; 2014.

18. Gries T, Veit D, Wulfhorst B. Textile Fertigungsverfahren: Eine Einführung. Munich: Carl Hanser Verlag GmbH Co KG; 2018.

19. Birkefeld K, Röder M, von Reden T, Bulat M, Drechsler K. Characterization of biaxial and triaxial braids: fiber architecture and mechanical properties. Appl Compos Mater. 2012;19(3):259–73.

20. Metzner C, Gessler A, Kaufmann J, Kroll L. Functionalized braids as potential solution or high performance CFRP structures. In: 2nd International MERGE Technologies Conference: IMTC. 2015. p. 37–44.

21. Gessler A, Maidl F. Method for producing fiber composite semi-finished products by means of a round braiding technique. US Patent No: 7,581,479. 2009.

22. Badie S, Dash A, Sohn YJ, Vassen R, Guillon O, Gonzalez-Julian J. Synthesis, sintering and effect of surface roughness on oxidation of submicron Ti_2AlC. J Am Ceram Soc. 2021;104:1669–88.

23. Wang J, Wang J, Li A, Li J, Zhou Y. Theoretical study on the mechanism of anisotropic thermal properties of Ti_2AlC and Cr_2AlC. J Am Ceram Soc. 2014;97(4):1202–8.

24. European Committee for Standardization. ENV 843-4:2005-Advanced technical ceramics - monolithic ceramics - mechanical properties at room temperature-part 4: Vickers, Knoop and Rockwell superficial hardness.

25. Börger A, Supancic P, Danzer R. The ball on three balls test for strength testing of brittle discs: stress distribution in the disc. J Eur Ceram Soc. 2002;22(9):1425–36.

26. Börger A, Supancic P, Danzer R. The ball on three balls test for strength testing of brittle discs: part II: analysis of possible errors in the strength determination. J Eur Ceram Soc. 2004;24(10–11):2917–28.

27. Sun ZM. Progress in research and development on MAX phases: a family of layered ternary compounds. Int Mater Rev. 2011;56(3):143–66.

28. Bai Y, He X, Wang R, Sun Y, Zhu C, Wang S, et al. High temperature physical and mechanical properties of large-scale Ti_2AlC bulk synthesized by self-propagating high temperature combustion synthesis with pseudo hot isostatic pressing. J Eur Ceram Soc. 2013;33(13–14):2435–45.

29. Smialek JL. Environmental resistance of a Ti_2AlC-type MAX phase in a high pressure burner rig. J Eur Ceram Soc. 2017;37(1):23–34.

30. Rao JC, Pei YT, Yang HJ, Song GM, Li SB, De Hosson JThM. TEM study of the initial oxide scales of Ti_2AlC. Acta Mater. 2011;59(13):5216–23.

31. Byeon JW, Liu J, Hopkins M, Fischer W, Garimella N, Park KB, et al. Microstructure and residual stress of alumina scale formed on Ti_2AlC at high temperature in air. Oxid Met. 2007;68(1–2):97–111.

32. Bermejo R. Towards seashells under stress: bio-inspired concepts to design tough and reliable ceramic components. J Eur Ceram Soc. 2017;37:3823–39.

33. Clegg W, Kendall K, Alford N, Button T, Birchall J. A simple way to make tough ceramics. Nature. 1990;347:455–7.

34. Weibull W. A Statistical distribution function of wide applicability. J Appl Mech. 1951;18:293–7.

35. Barsoum MW, El-Raghy T, Ali M. Processing and characterization of Ti_2AlC, Ti_2AlN and $Ti_2AlC_{0.5}N_{0.5}$. Metall Mater Trans A. 2000;31:1857–65.

36. Barsoum MW, Radovic M. Elastic and mechanical properties of the MAX phases. Annu Rev Mater Res. 2011;41(1):195–227.